Supplementary information

Molybdenum-catalysed electrochemical green ammonia synthesis from dinitrogen and water

Ryoichi Kanega[1*], Kazuya Arashiba[2], Erika Ishida[1], Chieko Suzuki[1], Mika Kusaba[3], Yuma Ishitobi[4], Yuki Shinohara[3], Akihiro Ohira[1], Yoshiaki Nishibayashi[2*]

[1]Research Institute for Energy Efficient Technologies, National Institute of Advanced Industrial Science and Technology, Tsukuba Central 5, 1-1-1 Higashi, Tsukuba, Ibaraki, 305-8565, Japan
[2]Department of Applied Chemistry, School of Engineering, The University of Tokyo, Hongo, Bunkyo-ku, Tokyo 113-8656, Japan
[3]Advanced Technology Research Laboratories, Innovation Center, Idemitsu Kosan Co., Ltd., Kamizumi, Sodegaura, Chiba 299-0293, Japan
[4]Performance Materials Laboratories, Advanced Materials & Performance Chemicals Department, Advanced Materials Company, Idemitsu Kosan Co., Ltd., Anesakikaigan, Ichihara, Chiba 299-0193, Japan
*Correspondence: r-kanega@aist.go.jp, ynishiba@g.ecc.u-tokyo.ac.jp

Table of Contents

General Methods.

All manipulations were carried out under an atmosphere of Ar by using standard glove-box techniques unless otherwise stated. Electrochemical investigations were conducted using a Hokuto Denko HZ-Pro electrochemical measurement system. NH_3 was analyzed using ion chromatography (ECO IC, Metrohm) with a TSKgel SuperIC-Cation HSII (4.6 mm I.D.×10 cm) column. ^{1}H and ^{31}P NMR spectra were recorded on a Bruker Avance 400 spectrometer. Mass spectra were recorded on an Agilent LC/MSD iQ. $[MoI_3(PCP)]$ (**1a**; PCP = 1,3-bis((di-*tert*-butylphosphino)methyl)benzimidazol-2-ylidene)[S1], [Mo(N)I(PCP)] (**2a**)[S2], $[Mo(N)I(PCP^{CF3})]$ (**2b**; PCP^{CF3} = 1,3-bis((di-*tert*-butylphosphino)methyl)-5-(trifluoromethyl)benzimidazol-2-ylidene)[S2], 2,4,6-trimethylpyridinium trifluoromethanesulfonate ([ColH]OTf)[S3] were prepared according to the literature methods. The chemicals and carbon felt electrodes (AAF304ZS, Toyobo) were purchased from commercial suppliers and were used without further purification or treatment.

H_2 and O_2 quantification and faradaic efficiency (FE) calculation

H_2 and O_2 were quantified by gas chromatography (Shimadzu GC-8A) equipped with a thermal conductivity detector and a Molecular Sieve 5A column. Gas samples were collected periodically during electrolysis (0.1 mL for H_2 analysis and 0.5 mL for O_2 analysis), and the gas flow rate was measured simultaneously. Assuming that the gas flow rate and gas composition remained constant between sampling points, the total gas volume in each interval was estimated as $V_i = F_i \Delta t_i$, where $F_i$is the gas flow rate and $\Delta t_i$is the sampling interval. The amounts of H_2 and O_2 evolved in each interval were then calculated from the GC determined gas composition and V_i. The FE was calculated according to the following equation. Since it was difficult to distinguish N_2 crossover from the counter electrode from N_2 introduced by leakage during sampling, all detected N_2 was assumed to originate from leakage. The amount of O_2 produced was calculated by subtracting the corresponding leakage-derived O_2, estimated from the detected N_2, from the total detected O_2. F is the faradaic constant (96485 C mol^{-1}) and Q is the total charge passed during electrolysis.

$$\text{FE (\%)}: \frac{\mathrm{H_2}\ \text{(mol)} \times 2 \times F\ \text{(C mol}^{-1}\text{)}}{Q\ \text{(C)}} \times 100$$

$$\text{FE (\%)}: \frac{\mathrm{O_2}\ \text{(mol)} \times 4 \times F\ \text{(C mol}^{-1}\text{)}}{Q\ \text{(C)}} \times 100$$

a Electrochemical ammonia synthesis using TEMPO as a sacrificial electron source (**System 1**)

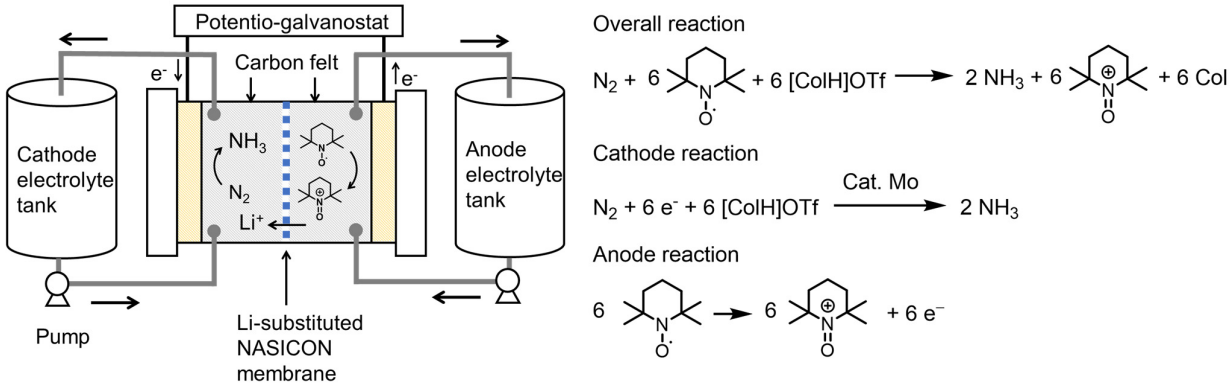

b Electrochemical ammonia synthesis using ethylene glycol as electron and proton sources (**System 2**)

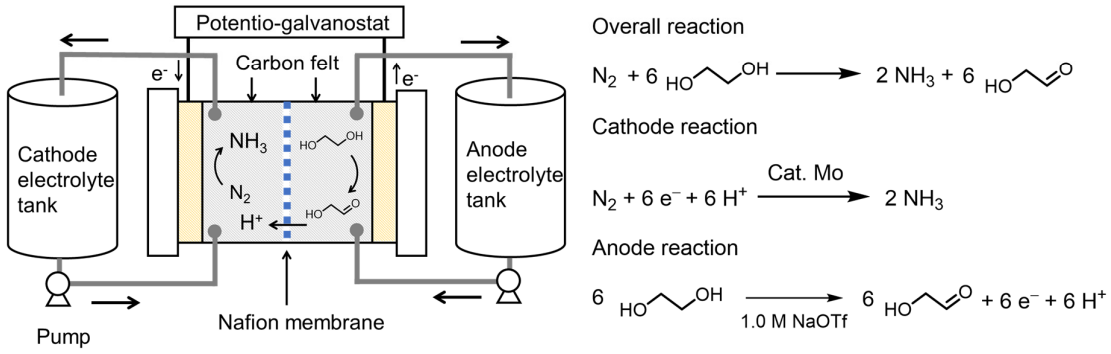

Supplementary Fig. 1 | Electrochemical ammonia synthesis with a flow-type electrochemical cell. a, Using TEMPO as a sacrificial electron source (**System 1**). **b**, Using ethylene glycol as electron and proton sources (**System 2**).

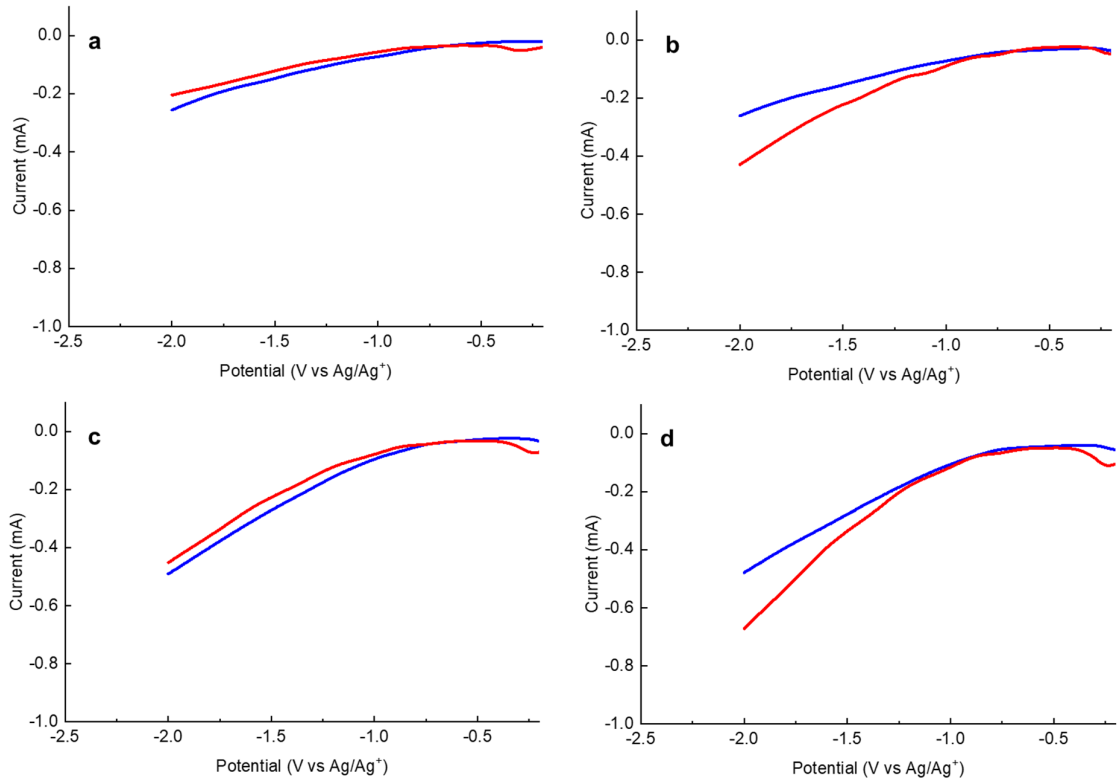

Supplementary Fig. 2 | Linear sweep voltammograms. Linear sweep voltammetry was conducted in 1.0 M LiOTf THF solution under Ar (blue) or N_2 (red) containing **a**, 1.0 mM **2a**, **b**, 1.0 mM **2a** and 1.0 mM [ColH]OTf, **c**, 1.0 mM **2b**, **d**, 1.0 mM **2b** and 1.0 mM [ColH]OTf.

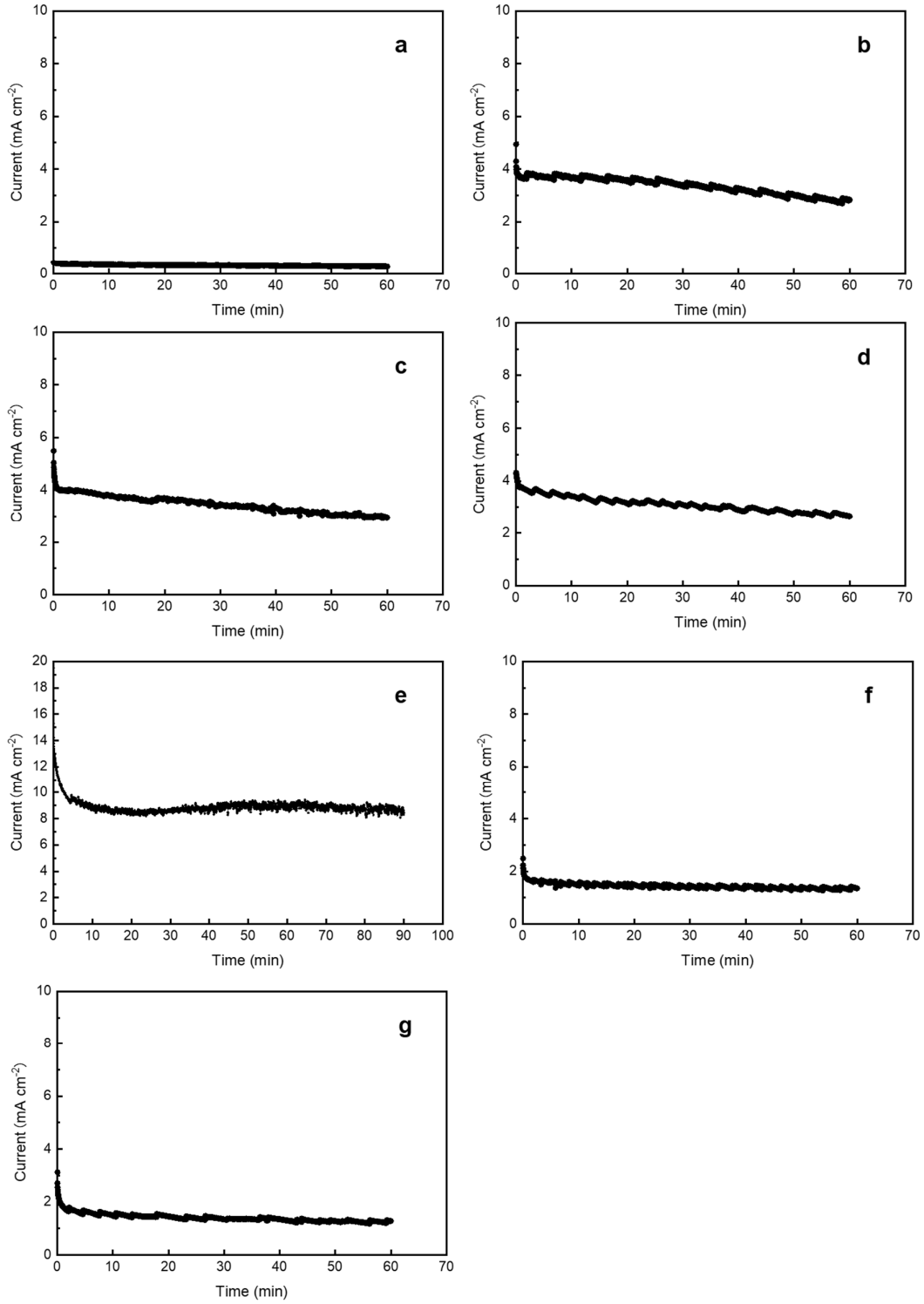

Supplementary Fig. 3 | Current density profiles corresponding to Table 1. a, at -0.5 V vs Ag/Ag^+ (Entry 2). **b**, at -0.8 V vs Ag/Ag^+ (Entry 1). **c**, at -1.2 V vs Ag/Ag^+ (Entry 3). **d**, at -1.5 V vs Ag/Ag^+ (Entry 4). **e**, optimized conditions (Entry 5). **f**, in the absence of **1a** (Entry 7). **g**, under Ar (Entry 8).

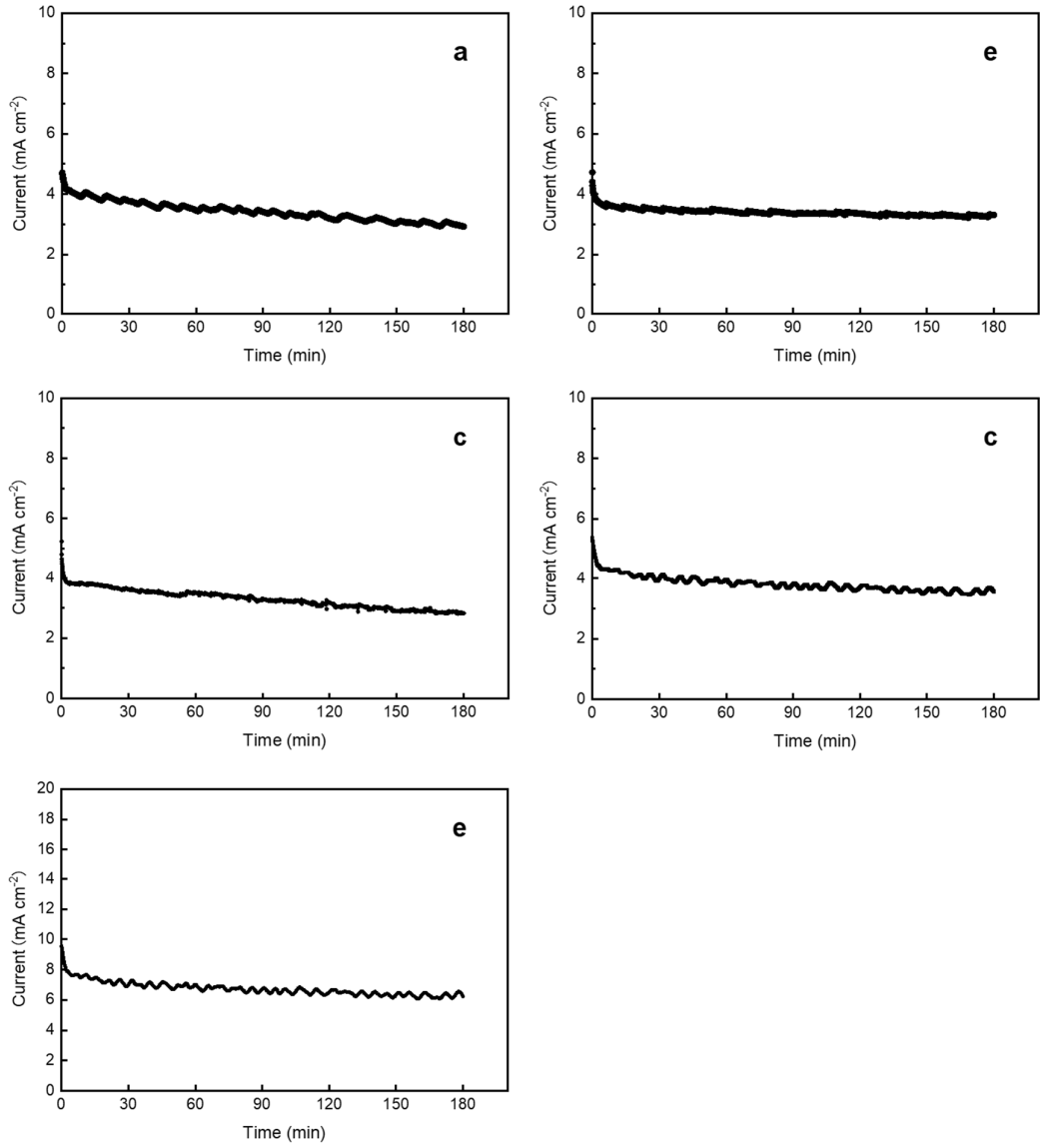

Supplementary Fig. 4 | Current density profiles in the presence of various concentrations of [ColH]OTf corresponding to Table 2. a, In the absence of [ColH]OTf (Entry 1). **b**, 2.5 mM (15 μmol, Entry 2). **c**, 10 mM (60 μmol, Entry 3). **d**, 30 mM (180 μmol, Entry 4). **e**, 100 mM (600 μmol, Entry 5).

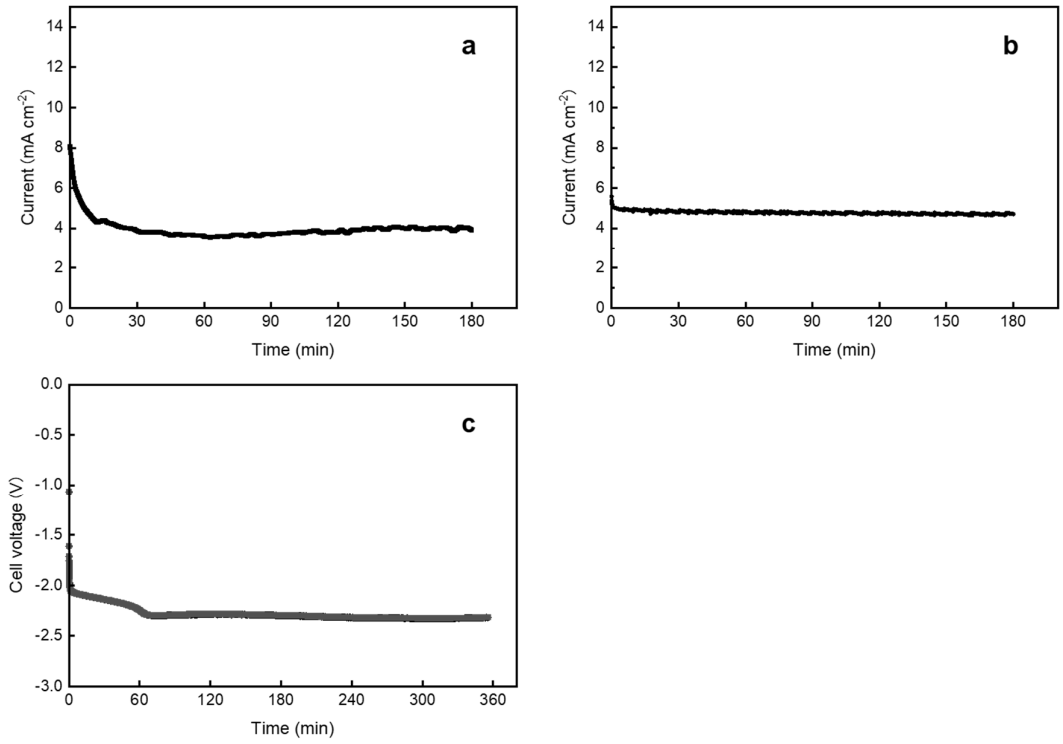

Supplementary Fig. 5 | Current density and cell voltage profiles corresponding to Table 2. a, In the presence of **2a** (Entry 6). **b**, In the presence of **2b** (Entry 7). **c**, galvanostatic electrolysis (Entry 8).

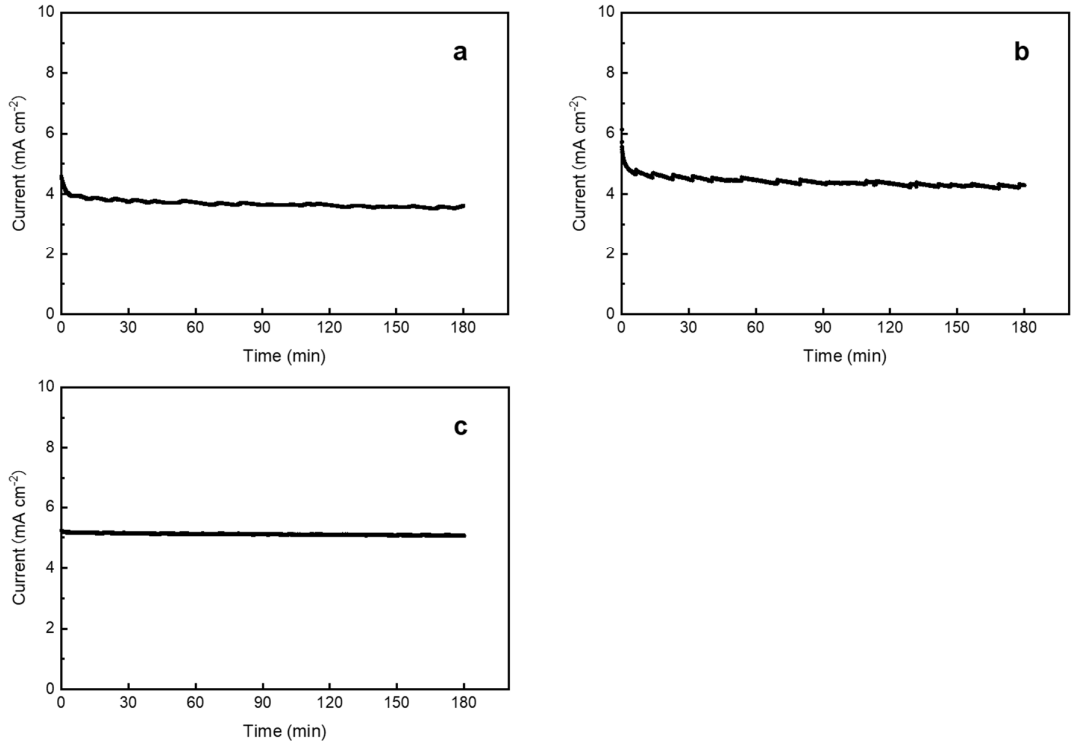

Supplementary Fig. 6 | Current density profiles with different electrolyte flow rates corresponding to Supplementary Table 1. a, At 5 mL min^{-1} (Entry 1). **b**, At 10 mL min^{-1} (Entry 2). **c**, At 40 mL min^{-1} (Entry 4).

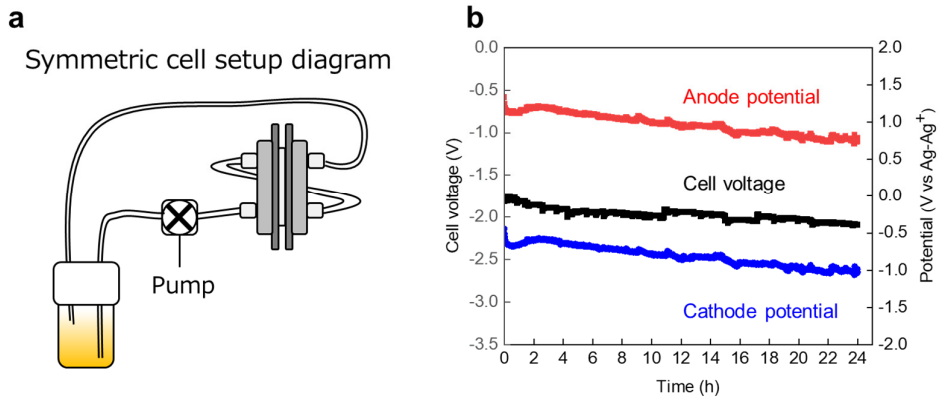

Supplementary Fig. 7 | Electrochemical durability test of 2b using a symmetric cell. a, Symmetric cell diagram. **b,** Cell voltage and potential profile. Electrolyte, **2b** and 1 M LiOTf in THF; separator, Poreflon（HPW-010-30); Electrode area, 2.5 cm^2; Electrolyte flow rate, 12.5 mL min^{-1}; N_2 flow rate, 2.5 mL min^{-1}; Current density, 10 mA cm^{-2}.

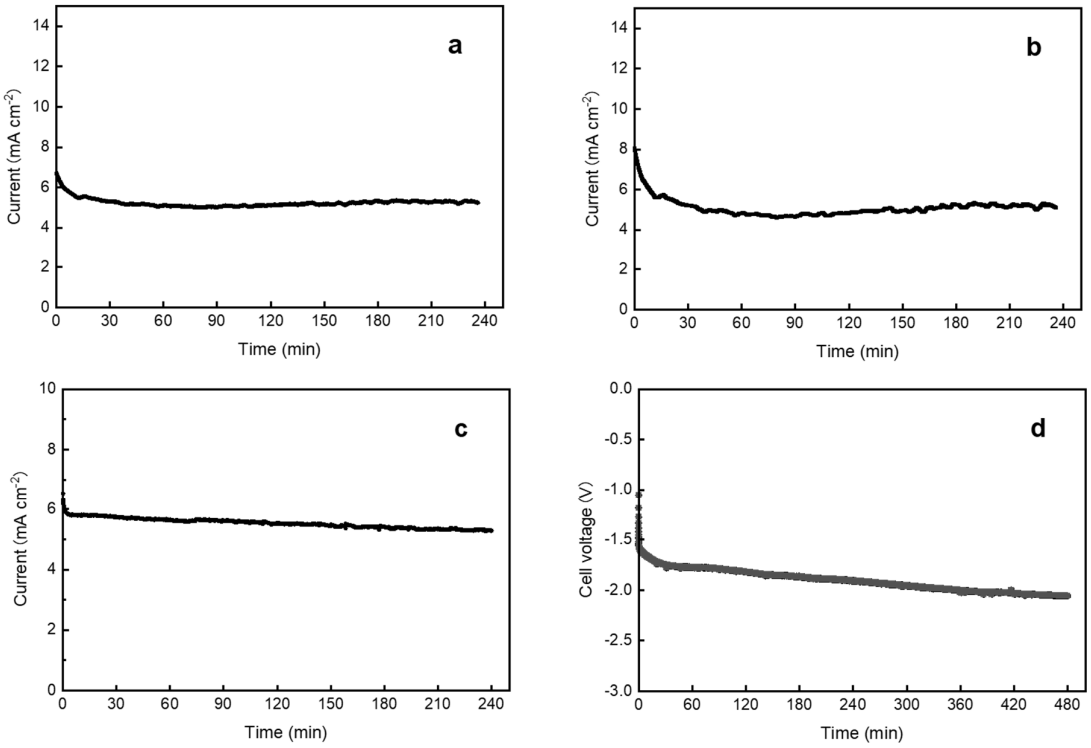

Supplementary Fig. 8 | Current density and cell voltage profiles corresponding to Table 3. a, In the presence of **1a** (Entry 1). **b**, In the presence of **2a** (Entry 2). **c**, In the presence of **2b** (Entry 3). **d**, galvanostatic electrolysis (Entry 4).

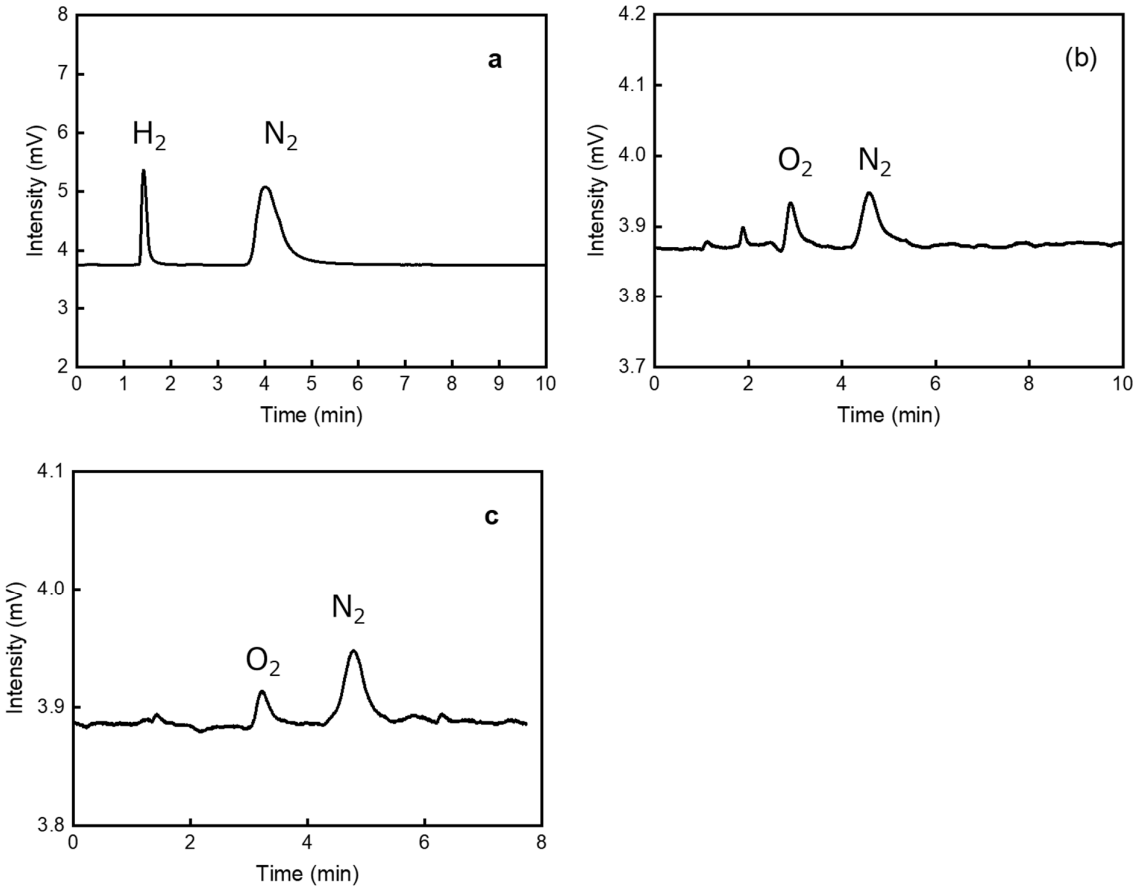

Supplementary Fig. 9 | Gas chromatograms for a, H_2, b, O_2 and c, Blank sample obtained before electrolysis.

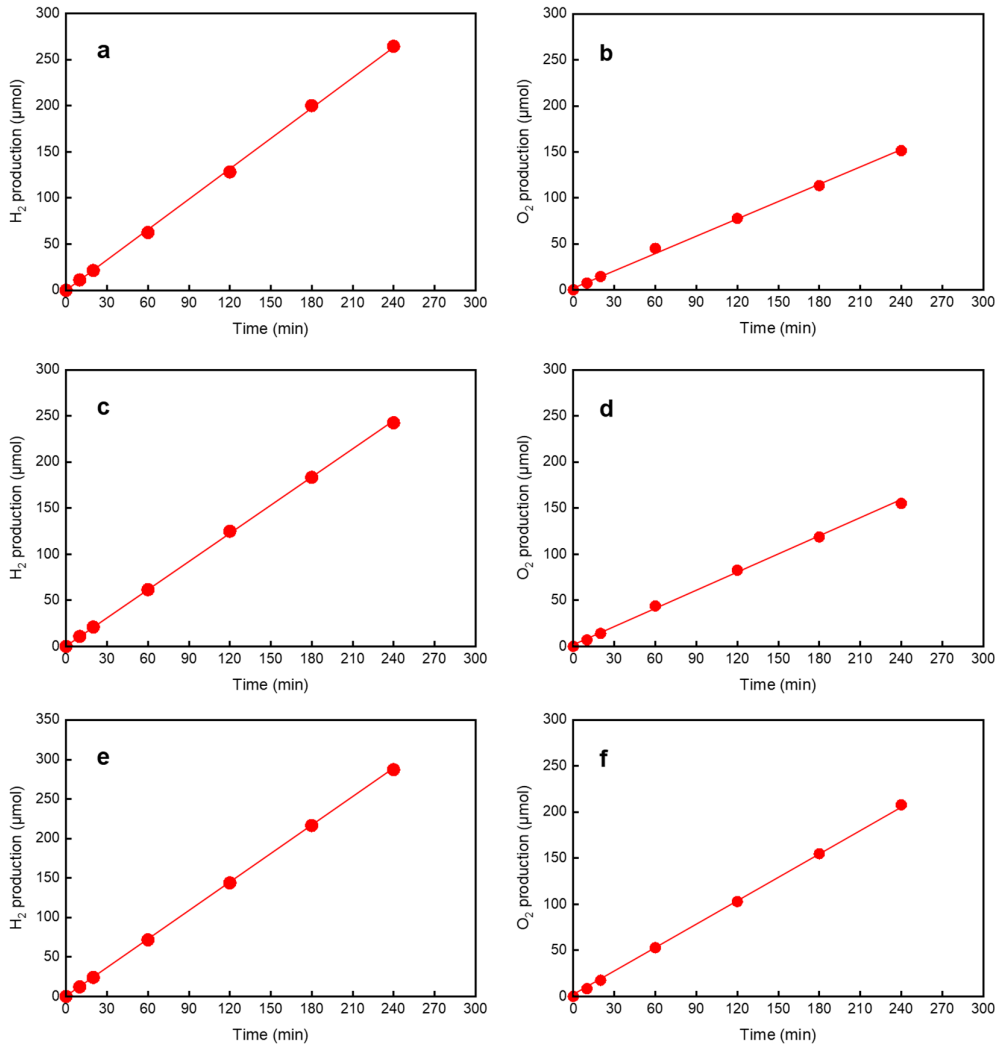

Supplementary Fig. 10 | Time course of H_2 and O_2 production with System 3 corresponding to Table 3. a, H_2 production in the presence of **1a** (Entry 1). **b**, O_2 production in the presence of **1a** (Entry 1). **c**, H_2 production in the presence of **2a** (Entry 2). **d**, O_2 production in the presence of **2a** (Entry 2). **e**, H_2 production in the presence of **2b** (Entry 3). **f**, O_2 production in the presence of **2b** (Entry 3).

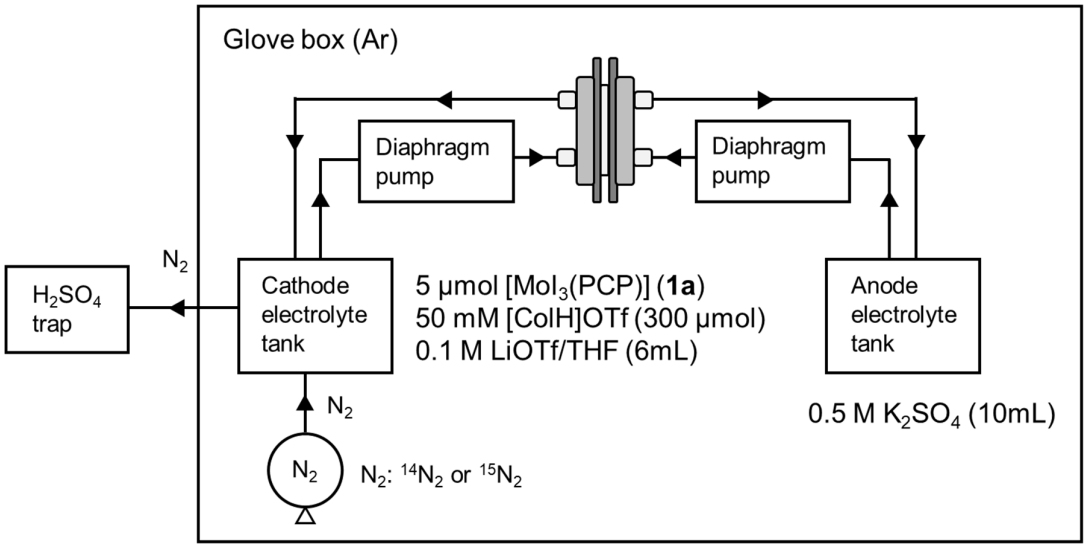

Supplementary Fig. 11 | Set up for an electrochemical NH_3 synthesis using $^{15}N_2$.

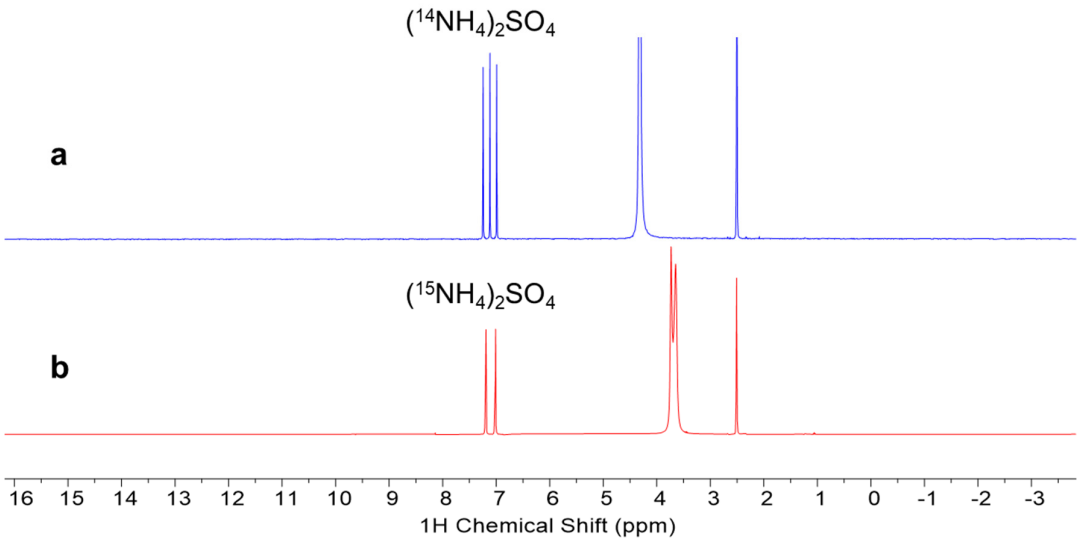

Supplementary Fig. 12 | ^{1}H NMR spectra (DMSO-d_6) of the volatile products obtained for Supplementary Fig. 11. a, Under $^{14}N_2$. **b**, Under $^{15}N_2$.

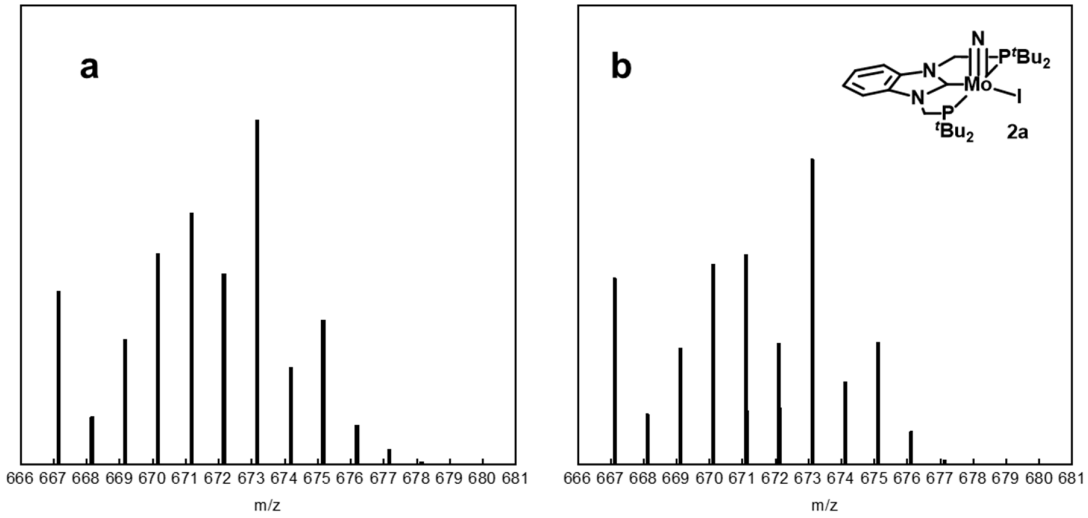

Supplementary Fig. 13 | a, Mass spectrum of the products obtained after electrolysis of [MoI_3(PCP)] **1a** under N_2. **b,** Calculated spectrum of [Mo(N)I(PCP)] **2a**.

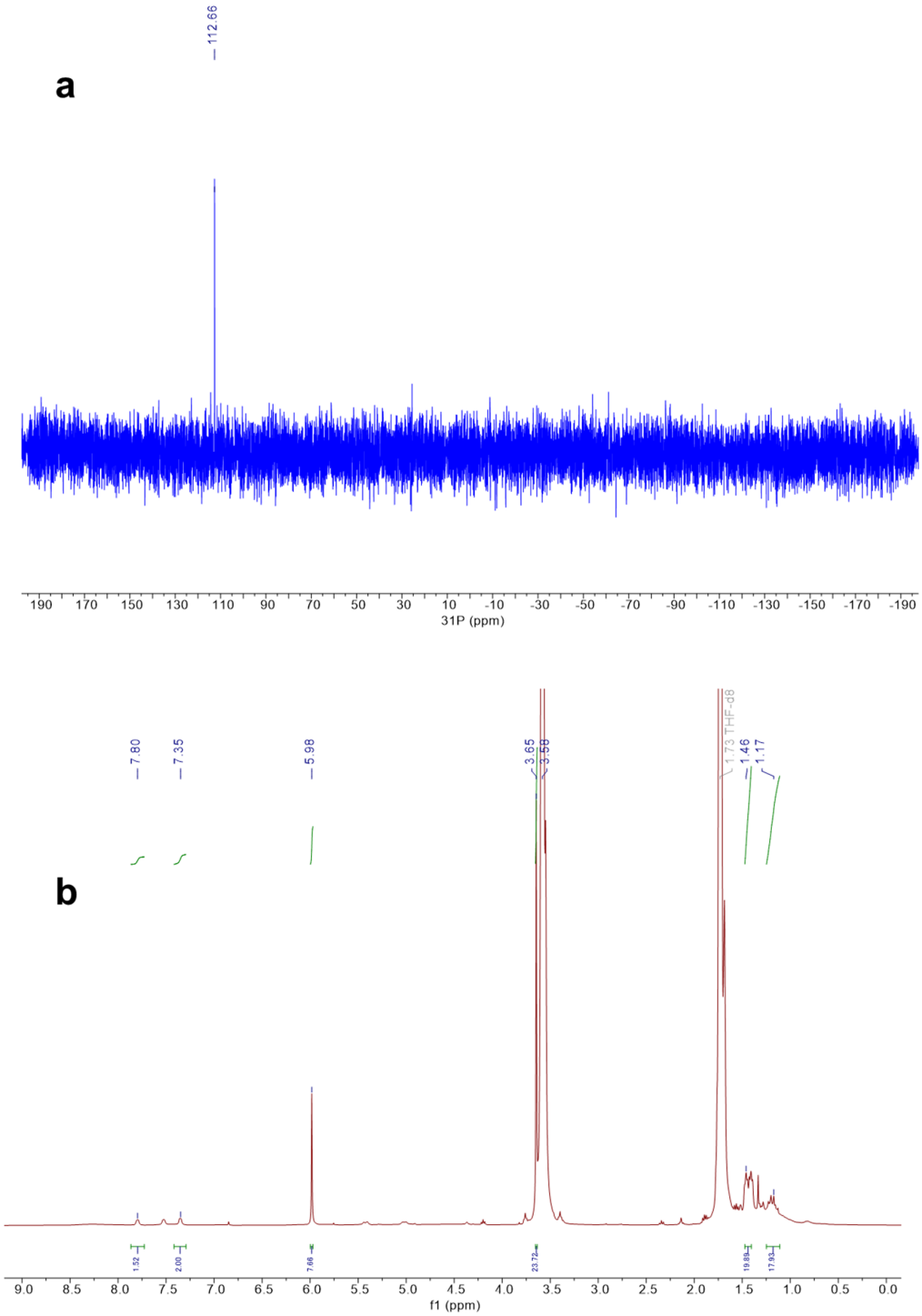

Supplementary Fig. 14 | a, ^{31}P and **b**, ^{1}H NMR spectra of the products obtained after electrolysis of **1a** under N_2.

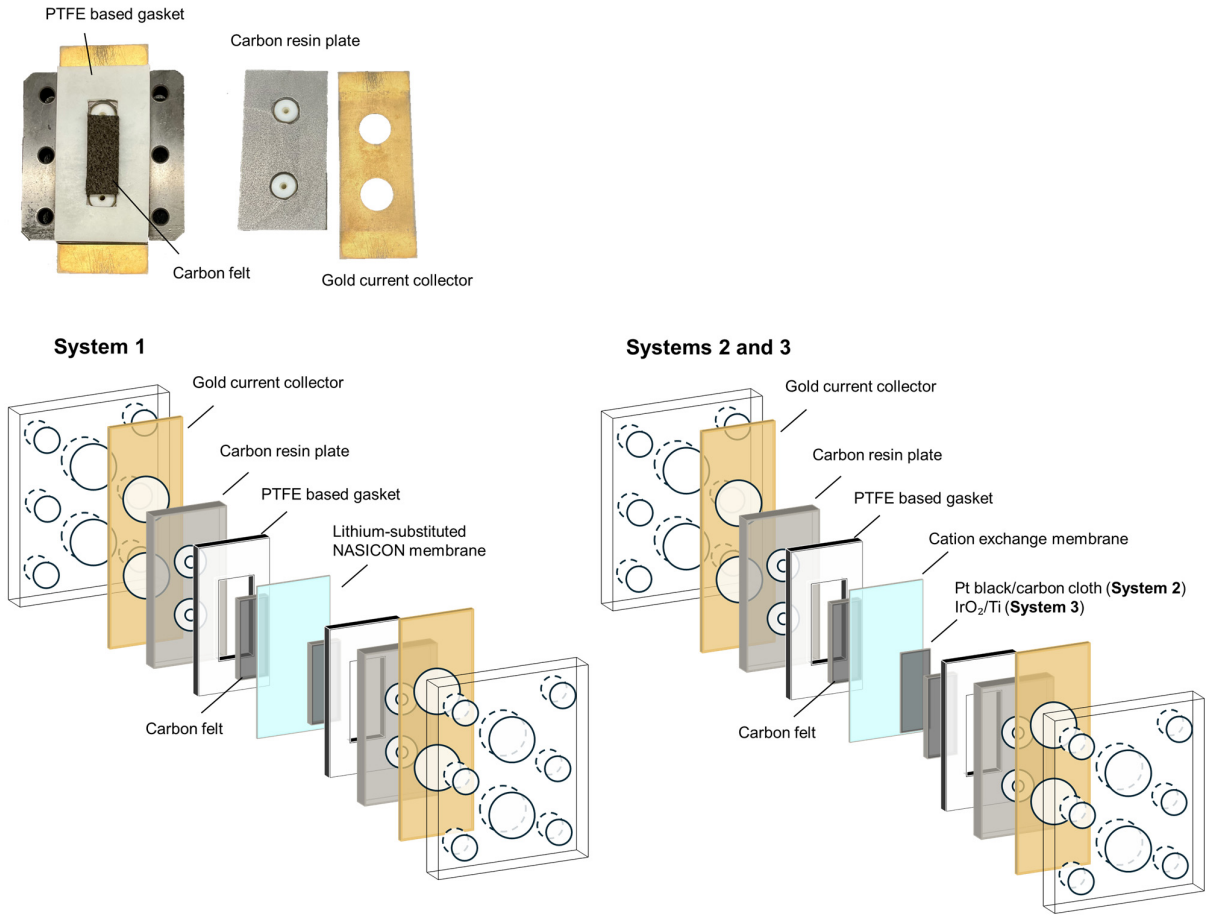

Supplementary Fig. 15 | Photograph of a flow cell for an electrochemical NH_3 synthesis. The flow cell was assembled by stacking a gold current collector, a carbon-resin plate and a 3 mm-thick PTFE-based gasket. A carbon felt electrode (Toyobo AAF304ZS) was placed inside the gasket, and the membrane was then placed on top of the electrode. The counter side was assembled in the same manner, and the cell was tightened with bolts.

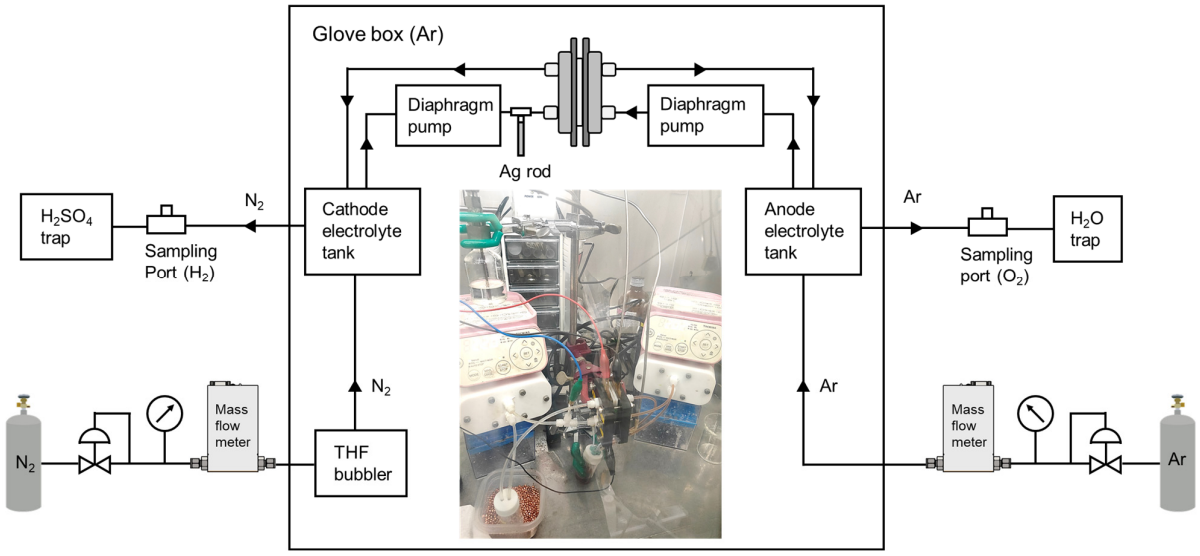

Supplementary Fig. 16 | Set-up of flow system for an electrochemical NH_3 synthesis. The cathode electrolyte was bubbled with N_2 for 10 min before electrolysis. The cathode and anode electrolytes were then circulated for 30 min to condition the membrane. After electrolyte circulation, electrolysis was carried out at the specified potential or current density.

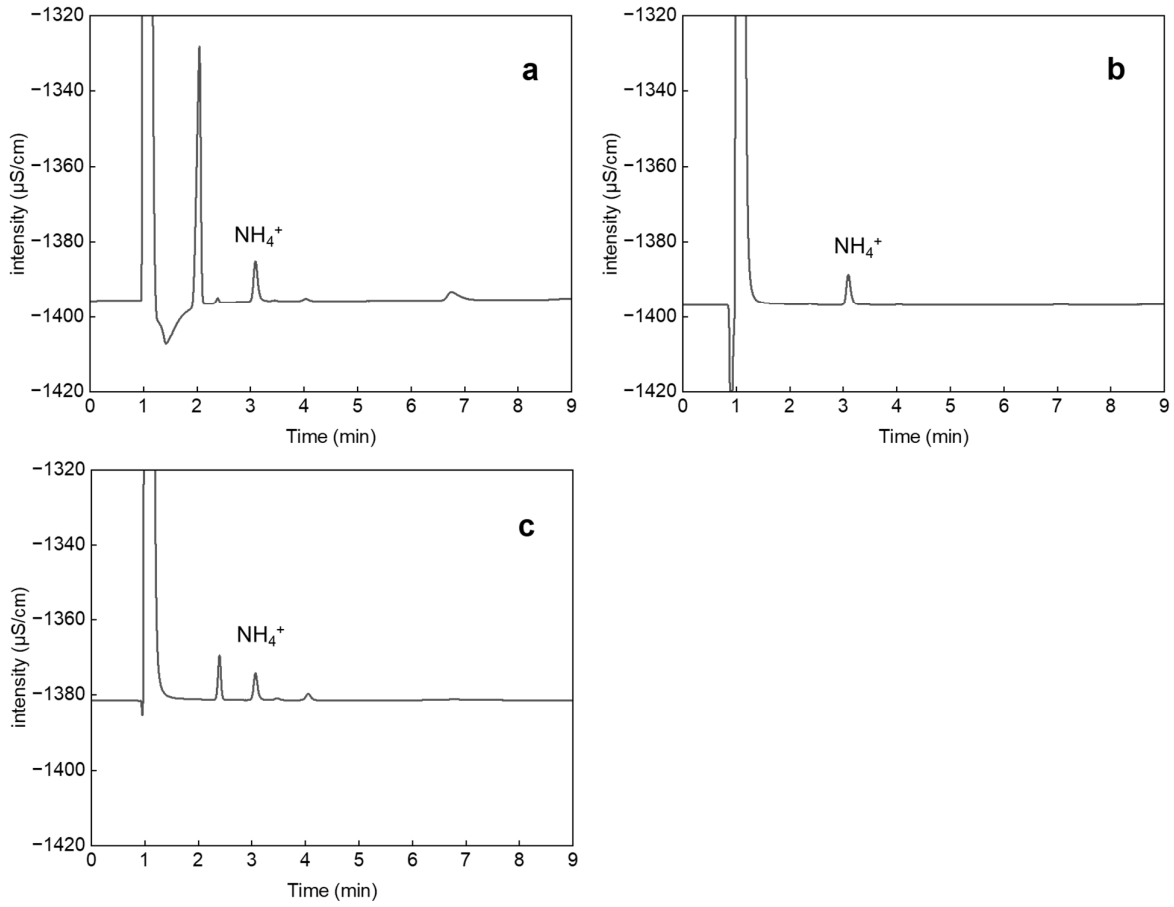

Supplementary Fig. 17 | Ion chromatograms of the products obtained for Table 3 (Entry 4). a, Cathode electrolyte. **b**, H_2SO_4 trap solution. **c**, 50 μM NH_4^+ standard solution.

Supplementary Table 1 | Effect of electrolyte flow rate on electrochemical NH_3 synthesis with System 2.

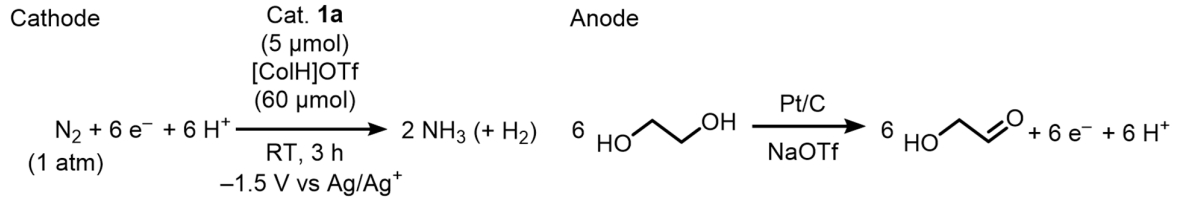

Entry	Electrolyte flow rate (mL min^{-1})	Average current density (mA cm^{-2})	NH_3 production (μmol)	NH_3 production (equiv. based on Mo)	FE (%)
1	5	3.0	20.5	4.1	14
2	10	3.3	23.8	4.8	15
3	20	3.8	26.5	5.3	14
4	40	3.9	10.2	2.0	5

Cathode electrolyte, 1.0 M LiOTf and 10 mM [ColH]OTf in THF (6 mL); anode electrolyte, 1.0 M NaOTf in ethylene glycol (6 mL); N_2 flow rate, 2.5 mL min^{-1}; separator, cation exchange membrane; applied potential, -1.5 V versus Ag/Ag^+; cathode, 1 × 1.3 cm; anode, 1 × 2.5 cm.

Supplementary Table 2 | NH_3 production and FE corresponding to Table 2 (Entries 8 and 9).

Entry	Time (h)	NH_3 production (μmol)	NH_3 production (equiv. based on Mo complex)	FE (%)
1	1	36.0	7.2	64
2	1	38.2	7.6	66
average		37.1 ± 1.6	7.4 ± 0.3	65 ± 1.4
3	2	78.3	16	63
4	2	83.2	17	67
average		80.8 ± 3.5	17 ± 0.7	65 ± 2.8
5	3	117.5	24	63
6	3	122.0	24	65
average		119.8 ± 3.2	24	64 ± 1.4
7	6	216.3	43	58
8	6	227.3	45	61
average		221.8 ± 7.8	44 ± 1.4	60 ± 2.1
9	18	537.1	107	48
10	18	549.5	109	49
average		543.3 ± 8.8	108 ± 1.4	49 ± 0.7

Errors represent standard deviations of two independent runs.

Supplementary Table 3 | Electrochemical NH_3 synthesis with System 3.

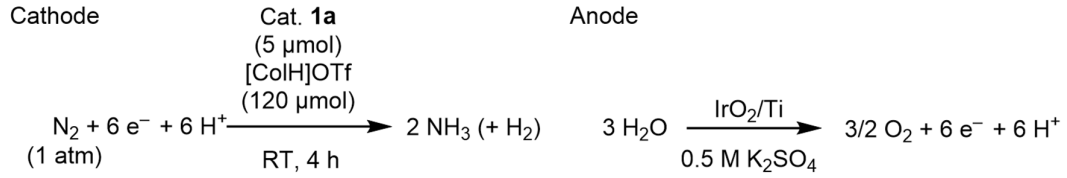

Entry	Cathode potential (V vs Ag/Ag^+)	Average current density ($mA\ cm^{-2}$)	NH_3 production (μmol)	NH_3 production (equiv. based on Mo complex)	Number of recycling of [ColH]OTf	FE (%)
1	-1.0	3.4	41.6	8.3	1.0	19
2	-1.2	4.0	58.3	12	1.5	23
3	-1.5	6.4	45.4	9.0	1.1	11

Cathode electrolyte, 0.5 M LiOTf and 20 mM [ColH]OTf in THF (6 mL); anode electrolyte, 0.5 M K_2SO_4 (10 mL); N_2 flow rate, 2.5 mL min^{-1}; electrolyte flow rate, 5 mL min^{-1}; separator, cation exchange membrane; cathode, 1 × 1.3 cm; anode, 1 × 2.5 cm.

Supplementary Table 4 | Production and FE of H_2 and O_2 corresponding to Table 3.

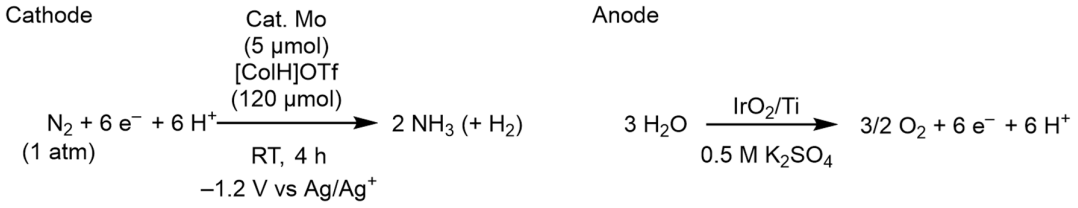

Entry	Cat. Mo	Average current density (mA cm^{-2})	NH_3 production (μmol)	FE (%)	H_2 production (μmol)	FE (%)	O_2 production (μmol)	FE (%)
1	**1a**	4.0	58.3	23	250.7	65	162.9	84
2	**2a**	3.9	64.8	26	242.5	64	155.1	82
3	**2b**	5.4	96.5	28	286.9	55	206.6	79

Cathode electrolyte, 0.1 M LiOTf and 20 mM [ColH]OTf in THF (6 mL); anode electrolyte, 0.5 M K_2SO_4 (6 mL); N_2 flow rate, 2.5 mL min^{-1}; electrolyte flow rate, 20 mL min^{-1}; separator, cation exchange membrane; applied potential, -1.2 V versus Ag/Ag^+; cathode, 1 × 1.3 cm; anode, 1 × 2.5 cm.

Supplementary Table 5 | Comparison of electrochemical NH_3 synthesis systems with uphill overall reactions using heterogeneous catalysts.

Entry	Catalyst	Electrolyte	FE (%)	Current density	Partial current density for NH_3 production	Ref.
1	Eex-COF/NC	0.1 M KOH	45	0.1 mA cm^{-2} at −0.2 V vs RHE	< 0.1 mA cm^{-2}	S4
2	GDY/Co_2N	0.1 M Na_2SO_4	59	0.5 mA cm^{-2} at 0.055 V vs RHE	0.2 mA cm^{-2}	S5
3	Co_{SC}-N-C	0.1 M KOH	52	0.5 mA cm^{-2} at −0.2 V vs. RHE	0.2 mA cm^{-2}	S6
4	Pd-GDY	0.1 M Na_2SO_4	32	0.25 mA cm^{-2} at −0.16 V vs. RHE	0.1 mA cm^{-2}	S7
5	Pd/HsGDY	0.05 M H_2SO_4	46	0.1 mA cm^{-2} at −0.25 V vs RHE	< 0.1 mA cm^{-2}	S8
6	F-doped carbon	0.05 M H_2SO_4	45	0.5 mA cm^{-2} at −0.3 V vs RHE	0.2 mA cm^{-2}	S9
7	PAL-MoS_2	0.1 M HCl	44	0.1 mA cm^{-2} at −0.1 V vs RHE	< 0.1 mA cm^{-2}	S10
8	BiNCs	0.5 M K_2SO_4	66	0.8 mA cm^{-2} at −0.6 V vs RHE	0.5 mA cm^{-2}	S11
9	Ru@ZrO_2/NC	0.1 M HCl	21	1.6 mA cm^{-2} at −0.21 V vs RHE	0.3 mA cm^{-2}	S12
10	Fe-SAs/LCC/GC	0.1 M KOH	31	0.25 mA cm^{-2} at −0.1 V vs RHE	0.1 mA cm^{-2}	S13
11	Fe/Co-O-C-1.0	0.1 M Na_2SO_4	70	1.5 mA cm^{-2} at −0.3 V vs. RHE	1.1 mA cm^{-2}	S14
12	**2b**	Cathode: 0.1 M LiOTf in THF Anode: 0.5 M K_2SO_4	39	5.0 mA cm^{-2}	2.0 mA cm^{-2}	This work

References

S1 Eizawa, A. *et al.* Catalytic Reactivity of Molybdenum–Trihalide Complexes Bearing PCP-Type Pincer Ligands. *Chem. Asian J.* **14**, 2091–2096 (2019). https://doi.org/10.1002/asia.201900496

S2 Ashida, Y. *et al.* Catalytic production of ammonia from dinitrogen employing molybdenum complexes bearing N-heterocyclic carbene-based PCP-type pincer ligands. *Nat. Synth.* **2**, 635–644 (2023). https://doi.org/10.1038/s44160-023-00292-9

S3 Arashiba, K. *et al.* Catalytic Reduction of Dinitrogen to Ammonia by Use of Molybdenum-Nitride Complexes Bearing a Tridentate Triphosphine as Catalysts. *J. Am. Chem. Soc.* **137**, 5666–5669 (2015). https://doi.org/10.1021/jacs.5b02579

S4 Liu, S. *et al.* Facilitating nitrogen accessibility to boron-rich covalent organic frameworks via electrochemical excitation for efficient nitrogen fixation. *Nat. Commun.* **10**, 3898 (2019). https://doi.org/10.1038/s41467-019-11846-x

S5 Fang, Y. *et al.* Graphdiyne Interface Engineering: Highly Active and Selective Ammonia Synthesis. *Angew. Chem. Int. Ed.* **59**, 13021–13027 (2020). https://doi.org/https://doi.org/10.1002/anie.202004213

S6 Liu, S. *et al.* Altering the rate-determining step over cobalt single clusters leading to highly efficient ammonia synthesis. *Natl. Sci. Rev.* **8** (2021). https://doi.org/10.1093/nsr/nwaa136

S7 Chen, Y. *et al.* Highly Productive Electrosynthesis of Ammonia by Admolecule-Targeting Single Ag Sites. *ACS Nano* **14**, 6938–6946 (2020). https://doi.org/10.1021/acsnano.0c01340

S8 Guo, Y. *et al.* Regulating nitrogenous adsorption and desorption on Pd clusters by the acetylene linkages of hydrogen substituted graphdiyne for efficient electrocatalytic ammonia synthesis. *Nano Energy* **86**, 106099 (2021). https://doi.org/https://doi.org/10.1016/j.nanoen.2021.106099

S9 Liu, Y. *et al.* A Highly Efficient Metal-Free Electrocatalyst of F-Doped Porous Carbon toward N_2 Electroreduction. *Adv. Mater.* **32**, 1907690 (2020). https://doi.org/https://doi.org/10.1002/adma.201907690

S10 Chen, J. *et al.* The activation of porous atomic layered MoS2 basal-plane to induce adjacent Mo atom pairs promoting high efficiency electrochemical N_2 fixation. *Appl. Catal. B* **285**, 119810 (2021). https://doi.org/https://doi.org/10.1016/j.apcatb.2020.119810

S11 Hao, Y.-C. *et al.* Promoting nitrogen electroreduction to ammonia with bismuth nanocrystals and potassium cations in water. *Nat. Catal.* **2**, 448–456 (2019). https://doi.org/10.1038/s41929-019-0241-7

S12 Tao, H. *et al.* Nitrogen Fixation by Ru Single-Atom Electrocatalytic Reduction. *Chem* **5**, 204–214 (2019). https://doi.org/https://doi.org/10.1016/j.chempr.2018.10.007

S13 Zhang, S. *et al.* Electrocatalytically Active Fe-(O-C2)4 Single-Atom Sites for Efficient Reduction of Nitrogen to Ammonia. *Angew. Chem. Int. Ed.* **59**, 13423–13429 (2020). https://doi.org/https://doi.org/10.1002/anie.202005930

S14 Zhang, S. *et al.* Atomically dispersed bimetallic Fe–Co electrocatalysts for green production of ammonia. *Nat. Sustain.* **6**, 169–179 (2023). https://doi.org/10.1038/s41893-022-00993-7